Rolling ferrofluid drop on the surface of a liquid

To cite this article: V Sterr *et al* 2008 *New J. Phys.* **10** 063029

View the article online for updates and enhancements.

New Journal of Physics

The open-access journal for physics

Rolling ferrofluid drop on the surface of a liquid

V Sterr[1,4]**, R Krauß**[2]**, K I Morozov**[3]**, I Rehberg**[2]**, A Engel**[1]
and R Richter[2,4]

[1] Institut für Physik, Carl von Ossietzky Universtität, 26111 Oldenburg,
Germany
[2] Experimentalphysik V, Universität Bayreuth, 95440 Bayreuth, Germany
[3] Institute of Continuous Media Mechanics, 1 Korolev Street, 614013 Perm,
Russia
E-mail: sterr@theorie.physik.uni-oldenburg.de and
reinhard.richter@uni-bayreuth.de

Abstract. We report on the controlled transport of drops of magnetic liquid, which are floating on top of a non-magnetic liquid layer. A magnetic field which is rotating in a vertical plane creates a torque on the drop. Due to surface stresses within the immiscible liquid beneath, the drop is propelled forward. We measure the drop speed for different field amplitudes, field frequencies and drop volumes. Simplifying theoretical models describe the drop either as a solid sphere with a Navier slip boundary condition, or as a liquid half-sphere. An analytical expression for the drop speed is obtained which is free of any fitting parameters and is well in accordance with the experimental measurements. Possible microfluidic applications of the rolling drop are also discussed.

[4] Authors to whom any correspondence should be addressed.

IOP Institute of Physics Φ DEUTSCHE PHYSIKALISCHE GESELLSCHAFT

Contents

1. Introduction

A tiny drop of magnetic fluid (MF) responds to magnetic fields in many ways—it is a 'world in a nutshell'. Typically, $1\,\mu$l of MF contains more than 10^{13} magnetic mono-domain particles, each with a diameter of around 10 nm, which are suspended in a carrier fluid like water or kerosene [1]. In the absence of an external magnetic field there is no long-range order in the MF, but when exposed to a static field the magnetic grains orient in part which results in a net magnetization. Application of a rotating magnetic field induces a torque on the suspended magnetic grains. Due to the viscous coupling of the particles to its surrounding carrier liquid angular momentum is transferred to the whole drop and an abundance of phenomena is observed.

In a series of experiments pioneered by Bacri *et al* [2] a magnetic drop was levitated in a surrounding liquid and exposed to a field rotating in the horizontal plane. For very small angular frequencies of the field an elongated drop follows the field rotation quasi-adiabatically with small phase lag [3]–[7]. In the limit of high angular frequency one observes for small magnetic fields an oblate spheroid, for intermediate values transient shapes, and for large fields an oblate spheroid with 'spiny starfish' appearance [2, 8, 9], for a review see [10].

Our setup, investigated in experiment and theory in this paper, differs from the above configuration in two points fundamentally: (i) the field is rotating in a plane *oriented vertically* and (ii) the drop of ferrofluid is floating *on top* of a layer of non-MF. The field configuration is borrowed from a recent experiment ('the magnetic pump'), where the magnetic torque drives a continuous flow of ferrofluid in an open duct [11, 12]. By replacing the ferrofluidic layer with a floating drop we are able to propel the drop with a constant translation velocity $\boldsymbol{v}_{\text{drop}}$ with respect to the liquid surface. Moreover, we could in principle manoeuvre the drop to arbitrary positions on the whole two-dimensional liquid layer by utilizing an additional alternating field in the y-direction. This is a new and promising technique for microfluidic applications.

Our theoretical model describes the ferrofluid drop first as a solid sphere with a Navier slip boundary condition at its surface, then as a liquid (half-)sphere with own inner flow field.
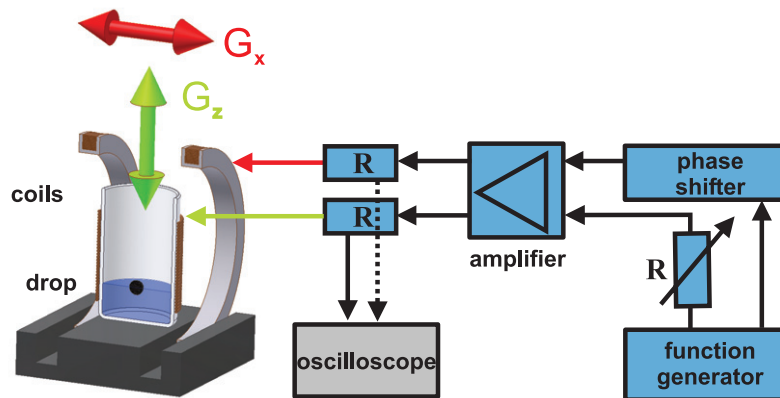
Figure 1. Sketch of the experimental setup. For details see text.

The problem is treated within Stokes approximation and the assumption of certain symmetries. In both cases an analytical expression for the drop speed v_{drop} in terms of the experimentally accessible parameters is obtained. While the solution of the Navier slip model contains an unknown parameter, the slip length, the result of the liquid half-sphere model is completely free of fitting parameters and is shown to represent the experimentally measured dependencies very well.

This paper is organized as follows: next we present the experimental arrangement together with some qualitative observations. This is followed by a comprehensive theoretical analysis (section 3). Subsequently the results obtained by the experiment and theory are compared in section 4 and discussed in section 5.

2. Experiment

Our experimental setup is shown in figure 1. We place a cylindrical glass beaker in between a Helmholtz pair of coils that produce an externally applied field $G_x(t)$ which is oriented horizontally. In addition, another coil is wrapped directly around the beaker providing a field $G_z(t)$ in the vertical direction. Here, we denote the external magnetic far field by $\boldsymbol{G}$ and the local one by $\boldsymbol{H}$. A sinusoidal driving current is supplied by connecting the output of a function generator (Fluke PM 5138A) to one channel of a power amplifier (Rotel RB-1090). The input of the second channel is supplied with a delayed signal of the function generator. In order to allow an independent adjustment of both currents, a variable resistor is inserted in one driving circuit. An oscilloscope serves to control the phase difference of both currents. When the phase difference is set to 90° the coils produce a rotating field $\boldsymbol{G}(t)$ inside the beaker. Any motion of the drop of magnetic liquid is observed from above by means of a video camera (not shown here).

For a good performance of the driving by the rotating field a large imaginary part of the susceptibility of the MF is important. Thus, we have selected a MF based on air stable cobalt particles [13], which are stabilized by oleic acid in kerosene. Figure 2 reproduces the frequency dependence of the complex susceptibility of this fluid measured by an ac-susceptometer [12]. The MF has a volume fraction of 5% and constitutes the interior (i) of the drop. Its viscosity was determined to be $\eta^{(i)} = 5.4\,\text{mPa\,s}$ by means of a low shear rheometer (Contraves LS40), and the density of the MF has been found to be $\rho^{(i)} = 1.07\,\text{g\,cm}^{-3}$.

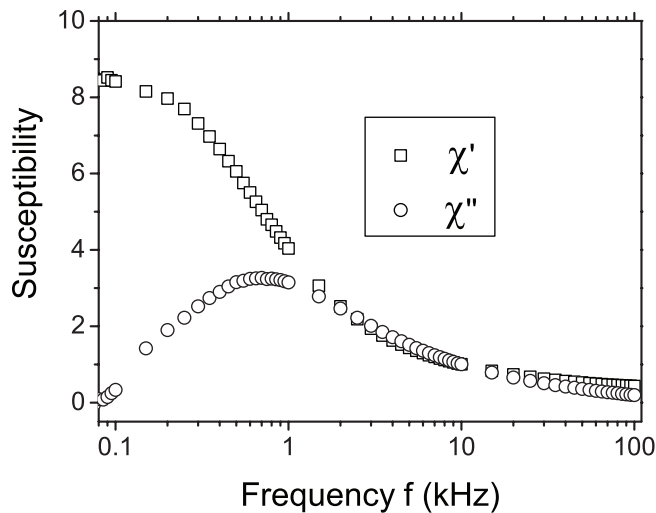**IOP** Institute of Physics Φ DEUTSCHE PHYSIKALISCHE GESELLSCHAFT

Figure 2. The magnetic susceptibility of the cobalt-based magnetic liquid versus the external alternating magnetic field. The data points for the real and imaginary parts of the susceptibility are marked by squares and circles, respectively.

The drop of MF has to float on top of a liquid layer of a non-MF. The quantities of this fluid outside of the drop will be marked by (o). This fluid must not mix with any of the components of the MF. Moreover, it must be denser than the MF. A per-fluorinated hydrocarbon fluid (Galden SV-90) proved a suitable substrate because of its higher density $\rho^{(o)} = 1.69\,\mathrm{g\,cm^{-3}}$, its long-term stability and its non-miscibility with the MF. According to the manufacturer the viscosity amounts to $\eta^{(o)} = 1.27\,\mathrm{mPa\,s}$, and the surface tension to $\gamma = 16\,\mathrm{mN\,m^{-1}}$. This fluid is poured into a cylindrical glass beaker up to a height of 2 cm in order to minimize fringe effects from the bottom of the glass.

At the beginning of an experiment a definite volume V of MF is put on the surface of the per-fluorinated liquid with a pipette. According to the density ratio of the two liquids approximately two-thirds of the volume of the forming drop is immersed (corresponding to a measured maximum penetration depth of about 60% of its diameter). The rotating field generated by the coils leads to a motion of the droplets in the direction the field is rolling. Hence the direction of the motion can be reversed by changing the sign of the phase difference between the ac-fields. Under the given experimental conditions we can achieve droplet velocities up to a few centimetres per second. The good contrast between the black MF and the transparent hydrocarbon liquid allows easy observation by a digital video camera. Snapshots from two exemplary movies can be seen in figure 3. The velocity of the droplets was determined by extracting the time a drop takes to travel a distance of 1 cm in the center of the beaker. Within this distance the magnetic field varies less than 1%.

3. Theory

The theoretical description of the 'real' setup poses a very complicated boundary value problem which would have to be solved by numerical methods. In order to extract the essence of the effect we make some simplifying assumptions which even lead to an analytical solution.

The droplet is considered to be a spherical object half-way immersed in a liquid with an otherwise perfectly flat surface. The liquid is assumed to be incompressible, so that the velocity
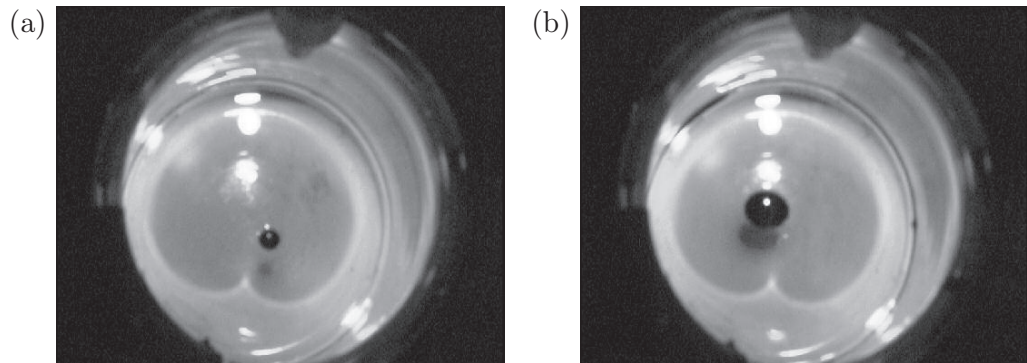
Figure 3. Drops of MF with a volume of (a) $5\,\mu$l (see movie 1) and (b) $80\,\mu$l (movie 2) rolling on top of a per-fluorinated Newtonian liquid. Both movies are available from stacks.iop.org/NJP/10/063029/mmedia.

field $\boldsymbol{v}$ obeys the equation of continuity

$$\nabla \cdot \boldsymbol{v} = 0. \tag{1}$$

Effects of gravity are neglected as is the inertia term in the Navier–Stokes equation which is hence rendered linear

$$\partial_t \boldsymbol{v} = -\nabla p + \eta \nabla^2 \boldsymbol{v}. \tag{2}$$

This Stokes approximation is in order when the Reynolds number Re is sufficiently small. Here it is given by $Re = \Omega R^2 \varrho^{(o)}/\eta^{(o)}$, with Ω the angular velocity of the sphere, and ranges between one and ten. The problem is treated within the reference frame where the sphere is rotating with its center at rest (cf figure 4), so that the basic equations are given by (1) and the stationary form of (2) which by eliminating the pressure p can be written as

$$\nabla^2 \left(\nabla \times \boldsymbol{v} \right) = \boldsymbol{0}. \tag{3}$$

In order to ensure stationarity in this frame, the overall forces and torques acting on the sphere must cancel out. After the velocity field of the surrounding liquid has been determined, its asymptotic value at $r \to \infty$ will give the negative translation velocity of the sphere in the laboratory frame.

The simplest approach is treating the droplet as a *solid* sphere and employing the common *no-slip* boundary condition at its surface, but this would lead to a logarithmically divergent viscous torque [14]. It has long been shown [15] that hydrodynamic problems containing a moving contact line in combination with the no-slip condition give rise to diverging quantities due to an inherent contradiction: on the one hand the fluid is supposed to stick to the solid surface, and yet the line where solid, liquid and gas meet shall advance on that very same surface.

Several means have been proposed to relieve the singularity, e.g. taking into account the strong curvature of the fluid surface near the solid, or describing the contact region in terms of molecular interactions, as has been done in [16]. A straightforward approach is to allow a certain amount of slippage over the solid surface. As early as 1823, a linear relation between the tangential stresses at a solid surface and the velocity of the latter was proposed by Navier [17]. Although other forms of slip condition can be successful [18, 19] this 'Navier slip' has become the most popular one and has since been examined and applied often. Earlier works
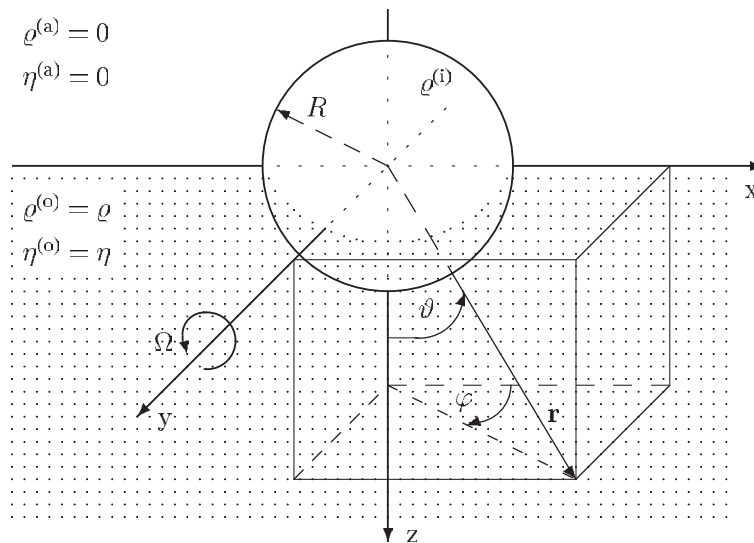
Figure 4. A spherical ferrofluid drop with radius R hosts in its inner (i) a fluid with density $\varrho^{(i)}$. It is covered from above (a) by a gas with density $\varrho^{(a)}$. The lower part of the drop is half-way immersed into an outer (o) Newtonian fluid with density $\varrho^{(o)}$ and dynamic viscosity $\eta^{(o)}$. The drop rotates with constant angular velocity Ω. The center of the sphere is the origin of the reference frame as indicated in the picture.

distinguish between several regions where different expansions are made, and only employ the slip condition in the contact region itself, finally matching the solutions together [20]–[22]. Our treatment, however, will follow the lines of O'Neill *et al* [23] who applied the Navier slip condition on the whole solid surface without seperating different regions. This is justified *a posteriori* by the fact that the slippage shows most of its impact in the direct vicinity of the contact line where the stresses are largest and leaves the flow field undisturbed further away, as will be made clear by the results of the present paper.

Although O'Neill *et al* [23] considered a problem quite analogous to ours, i.e. the rotation and translation of a solid spherical object which is half-way immersed in a liquid, we will present the treatment in a more lucid albeit less general way that will lead to a closed expression for the resulting flow field which is lacking in [23].

The disadvantage of the Navier slip condition is that it contains a characteristic length L_s which is supposed to be small compared to the length scales characterizing the problem (in our case the sphere radius R) and essentially indicates how much the fluid molecules slip over the solid surface. $L_s \to 0$ is equivalent to no slip, while $L_s \to \infty$ corresponds to completely unimpeded slip or zero tangential stress. This *slip length* does not necessarily 'represent true slippage but merely recognizes the fact that the liquid consists of molecules of finite size', as stated by Huh and Mason in [20]. Or as Cox puts it in [22]: 'Slip between liquid and solid is a convenient assumption to get rid of the non-integrable stress singularity'. Although the slip length between certain materials can now be measured (see e.g. [24]–[27]), this is of no use to the present problem, as the experiment does not involve a solid sphere.

By consequence, the result of these calculations will not be entirely satisfying, so that a second approach is taken in which the ferrofluid drop is treated as a *liquid half-sphere* with its own inner flow field. In this case, the velocity fields and also the sums of viscous and magnetic stresses must be continuous at the interface between the two liquids. Though the liquid drop cannot be described as a whole sphere but only as a half-sphere, the resultant drop speed, which no longer depends on any unknown parameters, represents the experimental data extremely well. This may indicate that the true flow field in the drop is mainly restricted to its lower part.

3.1. Solid sphere

The velocity field of the non-magnetic liquid bearing the sphere is expanded in vector spherical harmonics according to [28, 29]. Appendix A gives the details of this expansion and shows how the various coefficients occurring in it are determined from the boundary conditions.

When only one boundary condition is left, namely the requirement that the dissipating viscous torque compensates for the accelerating magnetic torque, the velocity components of the flow field below the sphere still depend on the yet unknown angular velocity Ω with which the sphere is rotating. The resulting expressions are (cf appendix A):

$$
\frac{v_r}{\Omega R} = \frac{1}{2} \frac{\cos\varphi \, \sin\vartheta}{1+2(L_s/R)} \left[1 - \frac{R^3}{r^3} \right]
$$
$$
+ \frac{1}{2}\cos\varphi \sum_{\substack{\ell=3 \\ \ell \, \text{odd}}}^{\infty} P_{\ell 1}(\cos\vartheta) \frac{R^\ell}{r^\ell} \left[1 - \frac{R^2}{r^2} \right] \frac{(-1)^{\frac{\ell-1}{2}}(2\ell+1)}{1+(2\ell+1)(L_s/R)} \cdot \frac{(\ell-2)!!}{(\ell+1)!!}
\tag{4}
$$

and

$$
\frac{1}{\Omega R}\begin{pmatrix} v_\vartheta \\ v_\varphi \end{pmatrix} = \frac{1}{2}\begin{pmatrix} \cos\varphi \, \cos\vartheta \\ -\sin\varphi \end{pmatrix}\left[1 + \frac{R^3}{2r^3} \right]\frac{1}{1+2(L_s/R)} + \frac{1}{2}\begin{pmatrix} \cos\varphi \, \partial_\vartheta \\ -\sin\varphi/\sin\vartheta \end{pmatrix}
$$
$$
\times \sum_{\substack{\ell=3 \\ \ell \, \text{odd}}}^{\infty} \frac{P_{\ell 1}(\cos\vartheta)\,(-1)^{\frac{\ell-1}{2}}}{1+(2\ell+1)(L_s/R)}\frac{R^\ell}{r^\ell}\left[(2-\ell) + \ell\frac{R^2}{r^2} \right]\frac{(2\ell+1)(\ell-2)!!}{\ell(\ell+1)(\ell+1)!!}
$$
$$
+ 2\begin{pmatrix} -\cos\varphi/\sin\vartheta \\ \sin\varphi \, \partial_\vartheta \end{pmatrix}\sum_{\substack{\ell=2 \\ \ell \, \text{even}}}^{\infty} \frac{P_{\ell 1}(\cos\vartheta)\,(-1)^{(\ell/2)}}{1+(\ell+2)(L_s/R)}\frac{R^{\ell+1}}{r^{\ell+1}}\frac{(2\ell+1)(\ell-3)!!}{\ell(\ell+1)(\ell+2)!!}.
\tag{5}
$$

The flow field determines the pressure via Stokes' equation (2). Straightforward calculation yields

$$
\nabla^2 \boldsymbol{v} = \nabla \sum_{\ell,m} \frac{2(2\ell-1)}{(\ell+1)}\frac{c_{\ell m}}{r^{\ell+1}}Y_{\ell m} = \frac{1}{\eta}\nabla p
\tag{6}
$$

so that the pressure field is given by

$$p(r, \vartheta, \varphi) = \eta \sum_{\ell, m} \frac{2(2\ell - 1)}{(\ell + 1)} \frac{c_{\ell m}}{r^{\ell + 1}} Y_{\ell m}(\vartheta, \varphi)$$

$$= \frac{3}{4} \eta \Omega \frac{\cos \varphi \, \sin \vartheta}{1 + 2(L_s/R)} \frac{R^2}{r^2}$$

$$+ \eta \Omega \cos \varphi \sum_{\substack{\ell = 3 \\ \ell \text{ odd}}}^{\infty} \frac{P_{\ell 1}(\cos \vartheta) \, (-1)^{\frac{\ell - 1}{2}}}{1 + (2\ell + 1)(L_s/R)} \frac{R^{\ell + 1}}{r^{\ell + 1}} \frac{4\ell^2 - 1}{\ell + 1} \frac{(\ell - 2)!!}{(\ell + 1)!!}. \quad (7)$$

3.2. Viscous torque

The viscous torque acting on the lower half-sphere is gained from the tangential viscous forces

$$\mathrm{d}\boldsymbol{F}_{\text{tang}} = [\sigma_{r\vartheta} \mathbf{e}_\vartheta + \sigma_{r\varphi} \mathbf{e}_\varphi] R^2 \mathrm{d}\varphi \, \mathrm{d}\vartheta \, \sin \vartheta \quad (8)$$

according to

$$\mathrm{d}\boldsymbol{T}_{\text{vis}} = \boldsymbol{R} \times \mathrm{d}\boldsymbol{F}_{\text{tang}}(r = R) \quad (9)$$

with the tangential components of the viscous stress tensor $\sigma_{r\vartheta}$ and $\sigma_{r\varphi}$ as defined in [30]. Integration over the lower half-sphere $0 \leqslant \vartheta \leqslant \pi/2$, $0 \leqslant \varphi \leqslant 2\pi$ yields the dimensionless viscous torque in the y-direction

$$\frac{-T_{\text{vis}}}{\pi \eta \, \Omega R^3} = \frac{3}{2} \frac{1}{1 + 2(L_s/R)} + \lim_{N \to \infty} \sum_{\substack{\ell = 3 \\ \ell \text{ odd}}}^{N} \frac{(2\ell + 1)^2}{1 + (2\ell + 1)(L_s/R)} \left[\frac{(\ell - 2)!!}{(\ell + 1)!!} \right]^2$$

$$+ \lim_{N \to \infty} \sum_{\substack{\ell = 2 \\ \ell \text{ even}}}^{N} \frac{4(2\ell + 1)(\ell + 2)}{1 + (\ell + 2)(L_s/R)} \left[\frac{(\ell - 3)!!}{(\ell + 2)!!} \right]^2. \quad (10)$$

When the doublefactorials in (10) are transformed to single factorials and Stirling's approximation

$$\ell! \approx \sqrt{2\pi \ell} \, \ell^\ell \mathrm{e}^{-\ell}, \qquad \ell \gg 1 \quad (11)$$

is employed, it can be shown that the terms for large ℓ in the infinite series give in leading order

$$\frac{2}{\pi \ell^2} \frac{R}{L_s}, \quad \text{for } L_s > 0, \quad (12)$$

$$\frac{4}{\pi \ell}, \qquad \text{for } L_s = 0. \quad (13)$$

While $\sum_{\ell=1}^{\infty} \ell^{-2}$ is a convergent series, $\sum_{\ell=1}^{\infty} \ell^{-1}$ diverges logarithmically, so here the necessity of the slip condition becomes manifest.

Looking at the solution (4) and (5) for the velocity field, it becomes clear that the field is only changed significantly near the contact line or, more generally, near the sphere surface: since $L_s \ll R$, which is a precondition for the validity of the Navier-slip model, the terms with
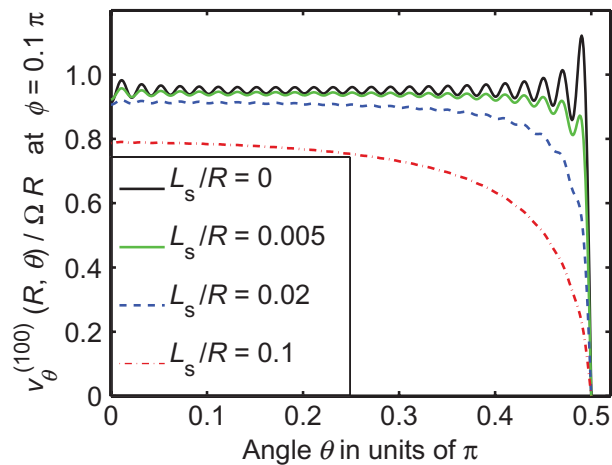
IOP Institute of Physics ⟨Φ⟩ DEUTSCHE PHYSIKALISCHE GESELLSCHAFT

Figure 5. Influence of slipping on $v_\vartheta^{(N)}(R)$ over ϑ for $N = 100$. Both the oscillations and the steep descent to zero are considerably smoothed out when a finite slip length is taken into account.
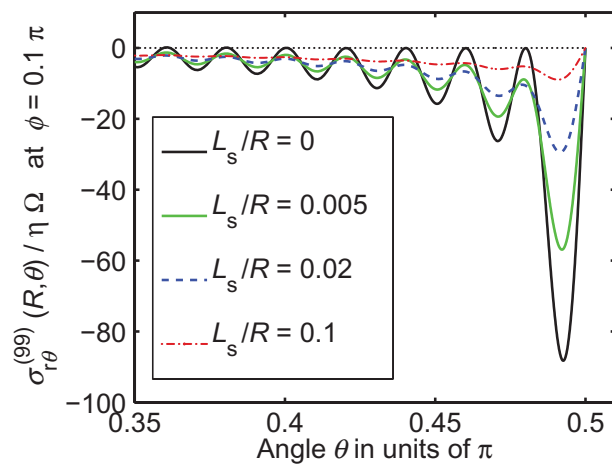

Figure 6. Influence of slipping on the relevant stress component $\sigma_{r\vartheta}^{(N)}(R)$ over ϑ for $N = 99$. The greater the slip length, the more the oscillations are damped, i.e. the more the stress is relieved.

small ℓ hardly deviate from those for no-slip. Within the $(\ell = 1)$-terms of equations (4), (5) and (10), the ratio L_s/R can safely be neglected. It is crucial, however, for the convergence of the series, for when $\ell L_s/R$ exceeds the order unity, the factors containing L_s become important. Each term is made smaller, and the more so the greater ℓ becomes and, of course, the greater the slip length. On the other hand, the terms with large ℓ, i.e. those which are influenced by the slip condition, are negligible when $r \gg R$. So the results with and without slippage would not be distinguishable far enough from the contact line.

Figures 5 and 6 illustrate the influence of slippage in the relevant region near $\vartheta = \pi/2$ for expansion orders 99 and 100, respectively. Where there is a steep descent in the dependence of $v_\vartheta^{(100)}(r = R)$ on ϑ and therefore a large corresponding tangential viscous stress $\sigma_{r\vartheta}^{(99)}(r = R)$ for $L_s = 0$, the curves are considerably smoothed out when the fluid is allowed to slip.

3.3. Magnetic torque

In order to obtain an expression for the angular velocity Ω, we utilize the fact that the viscous torque (10) must compensate for the magnetic torque which is calculated now.

The vector of the applied magnetic field rotates within the xz-plane, generating a torque in the y-direction, so that the external magnetic field is denoted by

$$\boldsymbol{G} = \mathfrak{Re}\{\hat{\boldsymbol{G}}\}, \qquad \hat{\boldsymbol{G}} = G\, e^{i\omega t}(-i\mathbf{e}_x + \mathbf{e}_z) \tag{14}$$

with $\omega = 2\pi f$ being the rotation frequency of the field and

$$\chi = \chi' - i\chi'' = \chi(f) \tag{15}$$

the frequency-dependent magnetic susceptibility of the sphere. Concerning the amplitude of the magnetic field, the susceptibility is assumed to be a constant.

The sphere is supposed to be magnetized homogeneously, having the overall magnetization (see for example sections 8 and 29 in [31])

$$\boldsymbol{M} = \mathfrak{Re}\{\hat{\boldsymbol{M}}\}, \qquad \hat{\boldsymbol{M}} = \frac{G\chi}{1 + (\chi/3)}\, e^{i\omega t}(-i\mathbf{e}_x + \mathbf{e}_z) \tag{16}$$

so that the magnetic torque acting on it in the stationary state is given by [1]

$$\boldsymbol{T}_{\mathrm{mag}} = \mu_0\, V\, \mathbf{e}_y\, (M_z G_x - M_x G_z) = \frac{4\pi}{3} R^3 \frac{\mu_0 G^2 \chi''}{(1 + (\chi'/3))^2 + (\chi''/3)^2}\, \mathbf{e}_y. \tag{17}$$

This must compensate for the viscous torque

$$\boldsymbol{T}_{\mathrm{vis}} = -\pi \eta\, \Omega R^3\, \Sigma(L_{\mathrm{s}})\, \mathbf{e}_y. \tag{18}$$

Here, the right-hand side of (10) is abbreviated by $\Sigma(L_{\mathrm{s}})$, reminding us that it includes an infinite series which depends on the slip length and cannot be computed analytically in closed form. The equality of viscous and magnetic torques poses the last boundary condition which makes sure that the rotational and, consequently, also the translational motion of the sphere is not accelerated, and finally gives the rotation frequency of the sphere:

$$\Omega = \frac{4}{3} \frac{\mu_0 G^2 \chi''}{\left[(1 + (\chi'/3))^2 + (\chi''/3)^2\right] \eta\, \Sigma(L_{\mathrm{s}})} \equiv \frac{8}{3} \frac{\mathfrak{M}}{\eta\, \Sigma(L_{\mathrm{s}})}. \tag{19}$$

The speed with which the sphere advances on the fluid surface is given by the negative of the velocity field at $r \to \infty$. In this limit, only the ($\ell = 1$)-terms remain. As has been explained above, the ratio L_{s}/R can be neglected in these terms, so that the drop speed reads

$$\boldsymbol{v}_{\mathrm{drop}} = -\frac{\Omega R}{2} \begin{pmatrix} \sin\vartheta\ \cos\varphi \\ \cos\vartheta\ \cos\varphi \\ -\sin\varphi \end{pmatrix} = -\frac{4}{3} \frac{\mathfrak{M}R}{\eta\, \Sigma(L_{\mathrm{s}})}\, \mathbf{e}_x. \tag{20}$$

3.4. Fluid (half-)sphere

Although a definite result has been obtained for the speed of the magnetic sphere, it cannot be compared to experimental data so easily. It still depends on an unknown parameter, the slip length L_{s}, which cannot be simply treated as a fit parameter. Due to the very weak dependence of the viscous torque on the expansion order, it poses a formidable numerical problem to obtain the slip length for a given torque, so it would be advantageous to obtain an expression for the drop speed that does not depend on such a parameter.
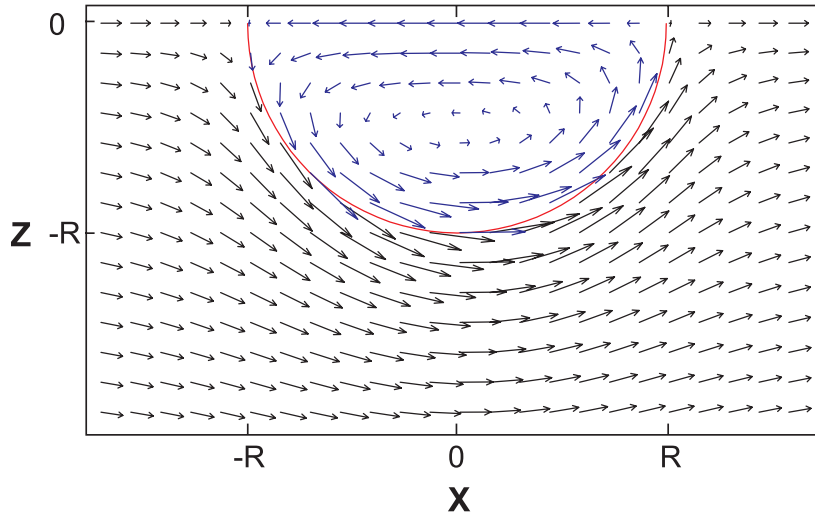
Figure 7. Flow field of the liquid half-sphere within the plane $y = 0$.

In addition, one could expect a model containing a *liquid drop* to be more realistic than the one with a *solid sphere*. For these reasons the ferrofluid drop is now considered liquid, though still spherical, being also subject to the hydrodynamic equations like the surrounding liquid. The Navier slip condition is replaced by the condition of continuous velocities and stresses at the interface between the two liquids. All other boundary conditions remain as before, including the addition of the mirror image. As a consequence of the requirement of a flat 'surface' ($v_\vartheta = 0$ at $z = 0$ for all $r > R$), it is not possible to obtain a spherical inner (i) velocity field: $v_\vartheta^{(i)}$ is rendered zero within the whole section $z = 0$ when the corresponding outer (o) component $v_\vartheta^{(o)}$ is demanded to vanish on the whole contact circle $z = 0$, $r = R$.

However, when the boundary conditions are posed in analogy to the previous section, a flow field is obtained which proves to be very useful. As the field becomes completely horizontal within the plane of symmetry, it is suggested that only the lower half-sphere is identified with the ferrofluid drop, i.e. after solving the mirror image setup, the whole upper half-space is neglected, resulting in the flow field displayed in figure 7.

The same differential equations (1), (3) and ansatz (A.7), (A.11) together with the requirement that the velocity be finite at $r = 0$ yield for the radial functions of the inner velocity field ($\ell > 0$):

$$f_{00}^{(i)}(r) \equiv 0, \tag{21}$$

$$f_{\ell m}^{(i)}(r) = q_{\ell m} r^{\ell+1} + B_{\ell m} r^{\ell-1}, \tag{22}$$

$$g_{\ell m}^{(i)}(r) = \frac{\ell+3}{\ell(\ell+1)} q_{\ell m} r^{\ell+1} + \frac{B_{\ell m}}{\ell} r^{\ell-1}, \tag{23}$$

$$h_{\ell m}^{(i)}(r) = p_{\ell m} r^\ell. \tag{24}$$

The starting points for the velocity components of the surrounding liquid are again the radial functions (A.19)–(A.24). For simplicity it is still assumed that the drop remains spherical, i.e.

$$v_r^{(i)}(R) = v_r^{(o)}(R) = 0, \qquad \forall \, \vartheta, \varphi, \tag{25}$$

instead of demanding that the normal stresses be continuous at $r = R$.

As mentioned above, the tangential components v_ϑ and v_φ must be continuous. Due to the orthogonalities (A.12) and (A.13) this condition reduces to the radial functions $g_{\ell m}$ and $h_{\ell m}$ being continuous.

Furthermore, the tangential forces must cancel out at every point on the spherical interface so that the tangential stresses are pointwise continuous. The latter consist of viscous stresses $\sigma_{r\vartheta/\varphi}^{(\text{vis})} \equiv \sigma_{r\vartheta/\varphi}$ and magnetic stresses [32]

$$\sigma_{ij}^{(\text{mag})} = \mu_0 H_i H_j - \frac{\mu_0}{2} H_i H_j \delta_{ij} + \frac{\mu_0}{2} (M_i H_j - M_j H_i), \tag{26}$$

where $i, j = x, y, z$ and the local magnetic field is given by

$$\boldsymbol{H} = \Re\{\hat{\boldsymbol{H}}\}, \qquad \hat{\boldsymbol{H}} = \frac{G}{1 + \frac{\chi}{3}} \, e^{i\omega t} \, (-i\boldsymbol{e}_x + \boldsymbol{e}_z), \tag{27}$$

assuming a linear magnetization law

$$\hat{\boldsymbol{M}} = \chi \hat{\boldsymbol{H}}. \tag{28}$$

The quantities $\boldsymbol{M}$, $\boldsymbol{G}$, χ and $\mathfrak{M}$ are defined as in the previous section. For the condition of continuous tangential stresses, the symmetric part of the magnetic stress tensor (26) need not be considered since it is the same on both sides of the interface due to the usual boundary conditions for $\boldsymbol{H}$.

The antisymmetric part, on the other hand, is the crucial one which leads to the propagation of the drop. It shall be denoted by $\sigma_{ij}^{(\text{m})}$. Because of antisymmetry in addition to $\hat{H}_y = \hat{M}_y = 0$, only one independent cartesian component is left:

$$\sigma_{xz}^{(\text{m})} = -\frac{\mu_0}{2} \frac{G^2 \chi''}{(1 + (\chi'/3))^2 + (\chi''/3)^2} = -\mathfrak{M}. \tag{29}$$

This gives the tangential magnetic stresses

$$\sigma_{r\vartheta}^{(\text{m})} = \mathfrak{M} \cos \varphi, \tag{30}$$

$$\sigma_{r\varphi}^{(\text{m})} = -\mathfrak{M} \cos \vartheta \sin \varphi. \tag{31}$$

Now the boundary condition reads

$$F_{\vartheta/\varphi}^{(\text{m})}(R) = F_{\vartheta/\varphi}^{(\text{vis,i})}(R) + F_{\vartheta/\varphi}^{(\text{vis,o})}(R) \tag{32}$$

because the accelerating magnetic force must be compensated by the viscous ones. With $F_{\vartheta/\varphi} = \sigma_{r\vartheta/\varphi} \, \boldsymbol{n} \cdot \boldsymbol{e}_r$ and the convention that the surface normal $\boldsymbol{n} = +\boldsymbol{e}_r$ for a force that acts on the *outer* surface and $\boldsymbol{n} = -\boldsymbol{e}_r$ for a force that acts on the *inner* surface, this yields in terms of stresses

$$\sigma_{r\vartheta/\varphi}^{(\text{m})} + \sigma_{r\vartheta/\varphi}^{(\text{vis,o})}(R) - \sigma_{r\vartheta/\varphi}^{(\text{vis,i})}(R) = 0 \tag{33}$$

for all ϑ, φ. As before, the viscous force in the x-direction must vanish. The resulting expressions of the components of inner and outer flow field are given explicitly in appendix B.

Again, the speed of the drop in the laboratory frame is obtained by evaluating the negative of the outer velocity field at $r \to \infty$, giving

$$\boldsymbol{v}_{\text{drop}}^{\text{liq}} = -\frac{1}{2} \frac{\mathfrak{M} R}{2\eta^{(\text{o})} + 3\eta^{(\text{i})}} \, \boldsymbol{e}_x. \tag{34}$$

Although this result looks very similar to the one obtained in the previous section,

$$\boldsymbol{v}_{\text{drop}}^{\text{sol}} = -\frac{4}{3} \frac{\mathfrak{M} R}{\eta^{(\text{o})} \Sigma(L_{\text{s}}) \, \mathbf{e}_x},$$ (35)

it clearly has two advantages. Firstly, it purely consists of parameters that are experimentally measurable or tunable (sphere radius R, viscosities η, and via $\mathfrak{M}$ susceptibility χ and external magnetic field amplitude G). Secondly, there is no need to calculate numerically an infinite sum.

Since no singularity has occurred in the scope of the calculations for the liquid sphere, it can be compared to a model where slipping is taken into account. The stresses which diverge within the framework of the very rigid no-slip condition are relieved both when the surrounding fluid is allowed to slip over the solid and when the solid is replaced by an elastic or, as in our case, viscous medium. Indeed, the crucial viscous stress component $\sigma_{r\vartheta}^{\text{liq}} \equiv \sigma_{r\vartheta}^{(\text{vis,o})}$ is essentially identical to the one obtained from the velocity field with Navier slip, the only differences being constant factors, at least when $\ell \gg 1$:

$$\frac{\sigma_{r\vartheta}^{\text{sol}}(R)}{\mathfrak{M}/\Sigma(L_{\text{s}})} = -\frac{4}{1+2L_{\text{s}}/R} \cos\varphi \cos\vartheta$$

$$-\frac{8}{3} \cos\varphi \sum_{\substack{\ell=3 \\ \ell \text{ odd}}}^{\infty} \partial_\vartheta P_{\ell 1}(\cos\vartheta) \, \frac{(-1)^{\frac{\ell-1}{2}}}{1/(2\ell+1)+L_{\text{s}}/R} \cdot \frac{(2\ell+1)(\ell-2)!!}{\ell(\ell+1)(\ell+1)!!}$$

$$+\frac{16}{3} \frac{\cos\varphi}{\sin\vartheta} \sum_{\substack{\ell=2 \\ \ell \text{ even}}}^{\infty} P_{\ell 1}(\cos\vartheta) \, \frac{(-1)^{(\ell/2)}}{1/(\ell+2)+L_{\text{s}}/R} \cdot \frac{(2\ell+1)(\ell-3)!!}{\ell(\ell+1)(\ell+2)!!},$$ (36)

$$\frac{\sigma_{r\vartheta}^{\text{liq}}(R)}{\mathfrak{M}} = -\frac{3}{2} \frac{1}{2+3\eta^{(\text{i})}/\eta^{(\text{o})}} \cos\varphi \cos\vartheta$$

$$-\frac{2\cos\varphi}{1+\eta^{(\text{i})}/\eta^{(\text{o})}} \sum_{\substack{\ell=3 \\ \ell \text{ odd}}}^{\infty} \partial_\vartheta P_{\ell 1}(\cos\vartheta) \, (-1)^{\frac{\ell-1}{2}} \frac{(2\ell+1)(\ell-2)!!}{\ell(\ell+1)(\ell+1)!!}$$

$$+2\frac{\cos\varphi}{\sin\vartheta} \sum_{\substack{\ell=2 \\ \ell \text{ even}}}^{\infty} \frac{P_{\ell 1}(\cos\vartheta) \, (-1)^{(\ell/2)}}{1+(\ell-1)/(\ell+2) \cdot \eta^{(\text{i})}/\eta^{(\text{o})}} \cdot \frac{(2\ell+1)(\ell-3)!!}{\ell(\ell+1)(\ell+2)!!}.$$ (37)

4. Comparison of the experimental and theoretical results

The main result of the theory for the drop speed (34) reads explicitly

$$v_{\text{drop}}^{\text{liq}} = -\frac{R}{4} \frac{\mu_0 G^2}{2\eta^{(\text{o})}+3\eta^{(\text{i})}} \cdot \frac{\chi''}{(1+(\chi'/3))^2+(\chi''/3)^2}.$$ (38)

It can easily be compared with the data obtained in the experiments. They have been measured following the procedure described in section 2. Figure 8 presents a plot of the drop velocity versus the magnetic field amplitude G for a driving frequency of $f = 0.8$ kHz. We have used a droplet of volume $V = 5 \, \mu$l, corresponding to a sphere of radius $R \approx 1.1$ mm, on top of the liquid layer. The measured velocities (marked by full circles) show a monotonous increase with G. The solid line gives the values of (38), taking into account the viscosities
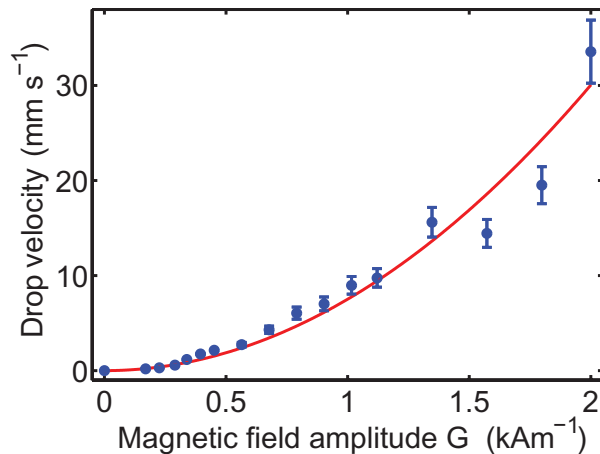
Figure 8. The drop speed in dependence of the magnetic field amplitude G for $f = 0.8\,\text{kHz}$ and $V = 5\,\mu\text{l}$. The blue circles mark the measured data, the red line gives the theoretical curve according to (38), taking into account the proper material values.
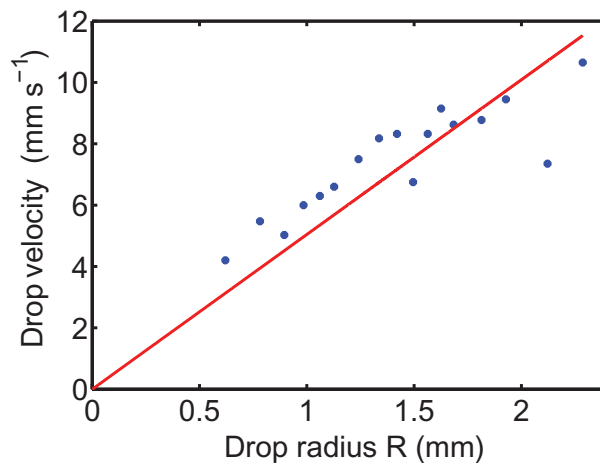

Figure 9. Drop velocity versus drop radius for an alternating magnetic far field with $G = 0.844\,\text{kA m}^{-1}$ and $f = 0.8\,\text{kHz}$. The blue dots mark the experimental results, the solid line the theoretical outcome.

of the ferrofluid, $\eta^{(\text{i})} = 5.4\,\text{mPa s}$ and of the liquid below, which amounts to $\eta^{(\text{o})} = 1.27\,\text{mPa s}$. The driving frequency enters into expression (38) only via the real and imaginary part of the magnetic susceptibility which were determined as $\chi' = 4.66$ and $\chi'' = 3.25$, respectively, for the given frequency (cf figure 2). As can be seen, the values for the liquid half-drop solution represent the given experimental data extremely well.

In a series of measurements, different drops with a volume ranging from 1 to $50\,\mu\text{l}$ were investigated. For comparison with the theory we assume a spherical symmetry and estimate the drop radius R from the drop volume V. As shown in figure 9, the measured drop velocity increases with the radius of the drops. The solid line marks the result of (38) for an amplitude of $G = 0.884\,\text{kA m}^{-1}$, as set in the experiment. Again we find a quantitative agreement of the half-drop solution with the experimental data.
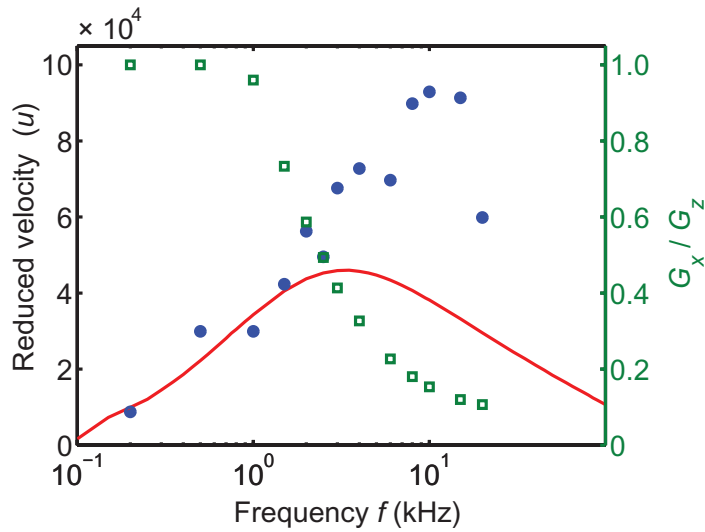
Figure 10. Frequency dependence of the reduced drop velocity u for $V = 5\,\mu$l. The full circles mark the experimental data, the solid line gives the theoretical curve where the measured frequency dependence of $\chi'(f)$ and $\chi''(f)$ has been plugged in. For all data G_z was fixed to $0.844\,\text{kA}\,\text{m}^{-1}$, but G_x was decreasing with increasing f. The green open squares indicate the actual ratio G_x/G_z.

As a further parameter the driving frequency f was varied in the experiment. When the frequency dependence of the drop speed was determined, the vertical field was fixed at $G_z = 0.844\,\text{kA}\,\text{m}^{-1}$. However, the frequency-dependent inductance of the outer coils did not permit G_x to be kept at this value for the whole range of frequencies (the ratio G_x/G_z is indicated on the rhs of figure 10). In order to obtain a magnitude which is independent of G, we introduce the reduced velocity

$$u = v_{\text{drop}}^{\text{liq}} \frac{\eta^{(\text{i})}}{R\mu_0 G_x G_z}, \tag{39}$$

where G_x denotes the horizontal- and G_z the vertical-field amplitude. Within the linear regime this quantity should be independent of the choice of the amplitudes. Figure 10 shows an increase of the reduced drop velocity (marked by solid circles) up to a maximum at $f = 10\,\text{kHz}$. The theoretical values (solid line) stem from (38), where the material parameters and the measured frequency dependence of the complex susceptibility $\chi'(f) + i\chi''(f)$, as presented in figure 2, have been utilized. In order to be able to compare the predictions with the experimental results, $v_{\text{drop}}^{\text{liq}}$ is scaled according to (39). We observe a good agreement up to a frequency of about $f = 1.5\,\text{kHz}$. Beyond that point, the theoretical curve deviates from the experimental results. The former shows a maximum at about $f = 3.5\,\text{kHz}$, while the measured velocity is largest at $f = 10\,\text{kHz}$, and the maximum values differ by a factor of two.

5. Discussion and conclusion

The measured propagation velocity of the droplet shows a parabolic dependence on the magnetic field amplitude, and a linear dependence on the radius of the droplet. Both experimental observations are quantitatively described by the liquid half-drop solution, without any free fitting parameter. The theory just needs the magnetic field amplitude, the complex susceptibility

and the viscosities of both fluids, i.e. the ferrofluid and the liquid layer. Taking into account the over-simplifying assumption of a half-spherical drop, the theory describes the experimental data remarkably well for driving frequencies up to 1.5 kHz.

For higher driving frequencies, however, (cf figure 10) a discrepancy between the experiment and theory of up to 100% is observed. This discrepancy may have several origins. Firstly, due to experimental characteristics, the rotating magnetic field becomes elliptical. Following [9], the nonlinear effects of an elliptical field are expected to diminish the flow within the droplet. This, however, does not explain our experimental data, which overcome the predictions by theory. Of course our experimental situation differs from that of [9] where an elliptical drop can freely rotate in the horizontal plane. In our case the horizontal surface pins the free rotation of an elliptical droplet in the vertical plane.

Secondly, for higher driving frequencies the liquid–liquid interface of a fully immersed drop develops spikes and resembles a 'spiny starfish', as reported in [2, 9]. This may also happen for the lower part of our half-immersed, floating drop. A complex interface of the two liquids may enhance the interaction between the fluids and thus increase the propulsion — similar to the paddle wheel of a Mississippi steam boat. This can of course not be covered by the simplifying model ansatz. The shape and dynamics of the liquid–liquid interface will be studied in forthcoming experiments.

The main achievement of this paper is that rotating fields can transport ferrofluidic drops. Our experimental results can be quantitatively explained without any free fitting parameters.

Moreover, the theory gives an explicit solution of the flow fields both for a rotating solid magnetic sphere and a spherical ferrofluid drop of which both are half-way immersed in a liquid. The similarity of the final results of both cases demonstrates the equivalence of Navier slip at a solid surface on the one hand and the continuity of tangential stresses at a fluid–fluid boundary on the other hand.

For a quantitative description of 'magnetic pumping' by means of a rotating field a droplet is more suitable than a plain ferrofluidic layer [12]. For the droplet one does not need any tracer particles (the droplet is its own tracer), and the demagnetization factor of an elliptical droplet is well defined.

Future experiments shall unveil whether the half-drop model also works in the pico-litre range. Here the dimensioning of droplets is very precise (see e.g. [35]) and their position may be detected by magnetic sensors [36]. Taking advantage of (38) one may even select the size of the generated droplets by their speed.

We propose that the controlled transport of small amounts of liquid to any desired position on top of a liquid two-dimensional layer is a promising technique for microfluidic applications. There ferrofluidic drops are commonly manipulated utilizing local field gradients, which are locally created by embedded wires [33] or planar coils [34]. In contrast, our driving technique yields a constant drop velocity globally, i.e. on the complete surface.

Acknowledgments

Appendix A. Explicit computation of the flow field below the solid sphere

The velocity field is expanded in vector spherical harmonics according to [28, 29]

$$\boldsymbol{v}(r, \vartheta, \varphi) = \sum_{\ell=0}^{\infty} \sum_{m=-\ell}^{+\ell} \{\mathbf{e}_r f_{\ell m}(r) + g_{\ell m}(r) r \nabla + h_{\ell m}(r) \boldsymbol{r} \times \nabla\} Y_{\ell m}(\vartheta, \varphi), \tag{A.1}$$

with the normalized spherical harmonics $Y_{\ell m}$ and the Legendre functions $P_{\ell m}$ as defined in [37] for $\ell \geqslant 0$ and $0 \leqslant m \leqslant \ell$:

$$Y_{\ell m}(\vartheta, \varphi) = (-1)^m \sqrt{\frac{2\ell+1}{4\pi} \frac{(\ell-m)!}{(\ell+m)!}} \times \mathrm{e}^{\mathrm{i}m\varphi} P_{\ell m}(\cos \vartheta), \tag{A.2}$$

$$\equiv K_{\ell m} \, \mathrm{e}^{\mathrm{i}m\varphi} P_{\ell m}(\cos \vartheta), \tag{A.3}$$

$$Y_{\ell,-m}(\vartheta, \varphi) = (-1)^m Y_{\ell m}^*(\vartheta, \varphi), \tag{A.4}$$

$$P_{\ell m}(\cos \vartheta) = \frac{(-1)^\ell}{2^\ell \ell!} (\sin \vartheta)^m \frac{\mathrm{d}^{\ell+m}}{\mathrm{d}(\cos \vartheta)^{\ell+m}} (\sin \vartheta)^{2\ell}. \tag{A.5}$$

When the expansion (A.1) is put into (1) and (3), these *partial* differential equations for the vector v are transformed to *ordinary* differential equations for the *scalar* radial functions $f_{\ell m}$, $g_{\ell m}$ and $h_{\ell m}$. Before this is done, equation (A.1) is simplified by several means.

With the Nabla operator in spherical coordinates

$$\nabla = \mathbf{e}_r \, \partial_r + \frac{1}{r} \mathbf{e}_\vartheta \, \partial_\vartheta + \frac{1}{r \sin \vartheta} \mathbf{e}_\varphi \, \partial_\varphi, \tag{A.6}$$

where $\partial_j \equiv \partial/\partial j$, the velocity components read:

$$v_r = \sum_{\ell=0}^{\infty} \sum_{m=-\ell}^{+\ell} f_{\ell m} Y_{\ell m}, \tag{A.7}$$

$$\begin{pmatrix} v_\vartheta \\ v_\varphi \end{pmatrix} = \sum_{\ell=0}^{\infty} \sum_{m=-\ell}^{+\ell} \left\{ g_{\ell m} \begin{pmatrix} \partial_\vartheta Y_{\ell m} \\ \frac{\mathrm{i}m}{\sin \vartheta} Y_{\ell m} \end{pmatrix} + h_{\ell m} \begin{pmatrix} -\frac{\mathrm{i}m}{\sin \vartheta} Y_{\ell m} \\ \partial_\vartheta Y_{\ell m} \end{pmatrix} \right\}. \tag{A.8}$$

With (A.4) and the fact that the velocity field is real valued it follows

$$g_{\ell,-m} = (-1)^m g_{\ell m}, \quad h_{\ell,-m} = (-1)^m h_{\ell m}. \tag{A.9}$$

Furthermore, when the symmetry of the problem with respect to the xz-plane, i.e.

$$v_\vartheta(-\varphi) = v_\vartheta(\varphi), \quad v_\varphi(-\varphi) = -v_\varphi(\varphi) \tag{A.10}$$

is taken into account, it can be shown with the aid of relations (A.4) and (A.9) that

$$\begin{pmatrix} v_\vartheta \\ v_\varphi \end{pmatrix} = \sum_{\ell=1}^{\infty} \sideset{}{'}\sum_{m=0}^{\ell} 2K_{\ell m} \left\{ g_{\ell m} \begin{pmatrix} \cos(m\varphi) \, \partial_\vartheta P_{\ell m} \\ \sin(m\varphi) \frac{-m}{\sin \vartheta} P_{\ell m} \end{pmatrix} - h_{\ell m} \begin{pmatrix} \cos(m\varphi) \frac{-m}{\sin \vartheta} P_{\ell m} \\ \sin(m\varphi) \, \partial_\vartheta P_{\ell m} \end{pmatrix} \right\}$$

$$\equiv 2 \sum_{\ell=0}^{\infty} \sum_{m=-\ell}^{+\ell} \{g_{\ell m} \boldsymbol{A}_{\ell m} + h_{\ell m} \boldsymbol{B}_{\ell m}\}. \tag{A.11}$$

The prime at the second sum indicates that the terms with $m = 0$ are divided by two.

When the boundary conditions are applied it will be important that the two velocity components of (A.11) are always considered together, because $\boldsymbol{A}_{\ell m} = \boldsymbol{A}_{\ell m}(\vartheta, \varphi)$ and $\boldsymbol{B}_{\ell m} = \boldsymbol{B}_{\ell m}(\vartheta, \varphi)$ fulfil the orthogonality relations

$$\langle \boldsymbol{A}_{\ell m}, \boldsymbol{B}_{\ell' m'} \rangle = 0, \tag{A.12}$$

$$\langle \boldsymbol{A}_{\ell m}, \boldsymbol{A}_{\ell' m'} \rangle = \langle \boldsymbol{B}_{\ell m}, \boldsymbol{B}_{\ell' m'} \rangle = \tfrac{1}{2}\ell(\ell+1)\delta_{\ell\ell'}\delta_{mm'} \tag{A.13}$$

with the vector inner product

$$\langle \boldsymbol{X}_1, \boldsymbol{X}_2 \rangle := \int_0^{2\pi} \mathrm{d}\varphi \int_0^{\pi} \mathrm{d}\vartheta \, \sin\vartheta \, (\boldsymbol{X}_1^*)^{\mathrm{T}} \boldsymbol{X}_2, \tag{A.14}$$

where * denotes the complex conjugate and $^{\mathrm{T}}$ the transpose of the vector. By computing the inner product of $\boldsymbol{A}_{\ell' m'}$ or $\boldsymbol{B}_{\ell' m'}$ with (A.11) one can reduce the infinite series to one function $g_{\ell' m'}(r)$ or $h_{\ell' m'}(r)$, respectively. If v_ϑ and v_φ were considered seperately, it would not be possible to get at the radial functions, because $\partial_\vartheta P_{\ell' m'}$ and $\pm\frac{\mathrm{i}m}{\sin\vartheta} P_{\ell m}$ alone are *not* orthogonal.

Now putting the expansions (A.7) and (A.11) into the basic equations (1) and (3) gives the following ordinary differential equations for the radial functions with $\ell > 0$ ($g_{00}(R) = h_{00}(R) \equiv 0$ can be assumed w.l.o.g.):

$$f_{00}' + \frac{2}{r} f_{00} = 0, \tag{A.15}$$

$$\frac{r}{\ell(\ell+1)} f_{\ell m}'''' + \frac{8}{\ell(\ell+1)} f_{\ell m}''' + \frac{2}{r}\left[\frac{6}{\ell(\ell+1)} - 1\right] f_{\ell m}'' - \frac{4}{r^2} f_{\ell m}' + \frac{1}{r^3}\left[\ell(\ell+1) - 2\right] f_{\ell m} = 0, \tag{A.16}$$

$$g_{\ell m}(r) = \frac{1}{\ell(\ell+1)}\left[r f_{\ell m}' + 2 f_{\ell m}\right], \tag{A.17}$$

$$h_{\ell m}'' + \frac{2}{r} h_{\ell m}' - \frac{\ell(\ell+1)}{r^2} h_{\ell m} = 0. \tag{A.18}$$

These equations are solved by a power law ansatz which together with the requirement that the velocity be finite as $r \to \infty$ leads to

$$h_{\ell m}(r) = \frac{a_{\ell m}}{r^{\ell+1}}, \qquad \ell > 0, \tag{A.19}$$

$$f_{00}(r) = \frac{d_{00}}{r^2}, \tag{A.20}$$

$$f_{1m}(r) = b_{1m} + \frac{c_{1m}}{r} + \frac{d_{1m}}{r^3}, \tag{A.21}$$

$$g_{1m}(r) = b_{1m} + \frac{c_{1m}}{2r} - \frac{d_{1m}}{2r^3} \tag{A.22}$$

and for $\ell > 1$:

$$f_{\ell m}(r) = \frac{c_{\ell m}}{r^\ell} + \frac{d_{\ell m}}{r^{\ell+2}}, \tag{A.23}$$

$$g_{\ell m}(r) = \frac{-1}{\ell(\ell+1)}\left[\frac{(\ell-2)c_{\ell m}}{r^\ell} + \frac{\ell d_{\ell m}}{r^{\ell+2}}\right]. \tag{A.24}$$

The coefficients $a_{\ell m}$, b_{1m}, $c_{\ell m}$ and $d_{\ell m}$ are determined by successively applying the remaining boundary conditions. In the following section, the ferrofluid drop will be treated as a solid sphere. Its angular velocity Ω is introduced as a parameter that will have to be determined by the equality of viscous and magnetic torques generated by the external field and the surrounding liquid.

It should be noted here that the orthogonality relations (A.12) and (A.13) would not be valid if the ϑ-integral within the scalar product (A.14) were only carried out up to $\vartheta = \pi/2$. On the other hand, the liquid only occupies the lower half-space in the given problem, so we perform a little trick in order to be able to integrate over the whole sphere, i.e. we take advantage of our equations being linear and employ the superposition principle by adding the *mirror image* of our problem with respect to the xy-plane (fluid above, void below the sphere). The problem can be solved in this way and the resulting flow field in the upper half-space is simply neglected in the end.

Within the framework of this 'mirror image construction' the following boundary conditions are employed:

- Navier slip at the sphere surface

$$\left[\partial_r - \frac{1}{R} \right] \begin{pmatrix} v_\vartheta \\ v_\varphi \end{pmatrix} \bigg|_{r=R} = \frac{1}{L_s} \left[\begin{pmatrix} v_\vartheta(r=R) \\ v_\varphi(r=R) \end{pmatrix} - \boldsymbol{U} \right] \tag{A.25}$$

with the slip length $L_s \ll R$ and the velocity $\boldsymbol{U}$ of the sphere surface

$$\boldsymbol{U} = \begin{cases} 0, & \text{for } \vartheta = \pi/2 \\ R\boldsymbol{\Omega} \times \mathbf{e}_r, & \text{for } \vartheta < \pi/2 \\ -R\boldsymbol{\Omega} \times \mathbf{e}_r, & \text{for } \vartheta > \pi/2 \end{cases} \tag{A.26}$$

implying

$$v_r(r=R) = 0. \tag{A.27}$$

- Flat 'interface':

$$v_\vartheta \left(\vartheta = \frac{\pi}{2} \right) = 0, \qquad \forall r \geqslant R. \tag{A.28}$$

- No resulting (viscous) force on the sphere:

$$F_i = \int_0^{2\pi} \mathrm{d}\varphi \int_0^{\pi/2} \mathrm{d}\vartheta \sin\vartheta \sum_j \sigma_{rj}(r=R) \, \mathbf{e}_j \cdot \mathbf{e}_i = 0 \tag{A.29}$$

with $i \in \{x, y, z\}$, $j \in \{r, \vartheta, \varphi\}$ and $\mathbf{e}_i$, $\mathbf{e}_j$ the unit vectors in the respective directions. The relevant components of the viscous stress tensor σ_{rj} are taken as defined in [30].

As is obvious from the given symmetry, only F_x will be different from zero and thereby determine the last coefficient.

Since the magnetic field only creates a torque but no linear force, this boundary condition provides the requirement of unaccelerated translational motion.

A.1. Applying the boundary conditions

The first coefficients are determined by the r-component of the Navier slip condition

$$v_r(R) = \sum_{\ell=0}^{\infty} \sum_{m=-\ell}^{+\ell} f_{\ell m}(R) \, Y_{\ell m}(\vartheta, \varphi) = 0 \tag{A.30}$$

and the orthogonality of the scalar spherical harmonics $Y_{\ell m}$ [38]:

$$f_{\ell m}(R) = 0 \qquad \forall \ell, m$$
$$d_{00} = 0,$$
(A.31)

$$\Rightarrow d_{1m} = -R^3 b_{1m} - R^2 c_{1m}$$
$$d_{\ell m} = -R^2 c_{\ell m}, \quad \ell > 1.$$
(A.32)

The coefficients $c_{\ell m}$ and $a_{\ell m}$ are obtained by applying the appropriate vector inner product to the ϑ- and φ-components of the Navier slip condition

$$\left[1 + \frac{L_s}{R} - L_s \partial_r\right] \sum_{\ell=1}^{\infty} \sum_{m=0}^{\ell}{}' 2K_{\ell m} \left[g_{\ell m}\begin{pmatrix} \cos(m\varphi)\partial_\vartheta \\ \sin(m\varphi)\frac{-m}{\sin\vartheta} \end{pmatrix} - h_{\ell m}\begin{pmatrix} \cos(m\varphi)\frac{-m}{\sin\vartheta} \\ \sin(m\varphi)\partial_\vartheta \end{pmatrix}\right]P_{\ell m}\Bigg|_R$$
$$= \begin{cases} 0 & \text{for } \vartheta = \pi/2 \\ R\Omega\left(\cos\varphi\,\mathbf{e}_\vartheta\right) - \cos\vartheta\sin\varphi\mathbf{e}_\varphi & \text{for } \vartheta < \pi/2 \\ -R\Omega\left(\cos\varphi\,\mathbf{e}_\vartheta\right) - \cos\vartheta\sin\varphi\mathbf{e}_\varphi & \text{for } \vartheta > \pi/2 \end{cases}$$
(A.33)

which is done here exemplary for the scalar product with $\boldsymbol{A}_{\ell' m'}(\vartheta, \varphi)$ as defined in (A.14). The orthogonalities of the sine and cosine functions yield

$$\left(1 + \frac{L_s}{R}\right)g_{\ell m}(R) - L_s g'_{\ell m}(R) = 0, \qquad \forall\, m \neq \pm 1$$
(A.34)

and

$$\left[\left(1 + \frac{L_s}{R}\right)g_{\ell m}(R) - L_s g'_{\ell m}(R)\right]\ell(\ell+1) = \pi\Omega R K_{\ell 1}\int_0^{\pi/2} \mathrm{d}\vartheta\sin\vartheta\left[\partial_\vartheta + \cot\vartheta\right]P_{\ell 1}(\cos\vartheta)$$
$$-\pi\Omega R K_{\ell 1}\int_{\pi/2}^{\pi} \mathrm{d}\vartheta\sin\vartheta\left[\partial_\vartheta + \cot\vartheta\right]P_{\ell 1}(\cos\vartheta).$$
(A.35)

Now from [38] one finds

$$\partial_\vartheta P_{\ell 1} + \cot\vartheta\, P_{\ell 1} = \ell(\ell+1)P_{\ell 0}$$
(A.36)

and

$$\int_0^1 \mathrm{d}u\, P_\ell(u) = \int_{-1}^0 \mathrm{d}u\, P_\ell(u), \qquad \ell \text{ even,}$$
(A.37)

$$\int_0^1 \mathrm{d}u\, P_\ell(u) = -\int_{-1}^0 \mathrm{d}u\, P_\ell(u) = (-1)^{\frac{\ell-1}{2}}\frac{(\ell-2)!!}{(\ell+1)!!}, \qquad \ell \text{ odd}$$
(A.38)

so that with the definition of $K_{\ell m}$ according to (A.3) one obtains

$$\left[\left(1 + \frac{L_s}{R}\right)g_{\ell 1}(R) - L_s g'_{\ell 1}(R)\right] = 0, \qquad \forall \ell \text{ even}$$
(A.39)

and for odd ℓ

$$\left[\left(1 + \frac{L_s}{R}\right)g_{\ell 1}(R) - L_s g'_{\ell 1}(R)\right] = \Omega R\sqrt{\frac{(2\ell+1)\pi}{\ell(\ell+1)}}(-1)^{\frac{\ell+1}{2}}\frac{(\ell-2)!!}{(\ell+1)!!}.$$
(A.40)

With (A.22) and (A.24) this gives in detail

$$b_{10}\left[\frac{3}{2} + 3\frac{L_s}{R}\right] + \frac{c_{10}}{R}\left[1 + 3\frac{L_s}{R}\right] = 0, \tag{A.41}$$

$$b_{1,\pm1}\left[\frac{3}{2} + 3\frac{L_s}{R}\right] + \frac{c_{1,\pm1}}{R}\left[1 + 3\frac{L_s}{R}\right] = \mp\Omega R\sqrt{\frac{3\pi}{2}}, \tag{A.42}$$

$$c_{\ell m} = 0, \quad \forall\, m \neq \pm1.$$

$$c_{\ell,\pm1} = 0, \quad \forall\, \ell \text{ even,}$$

$$c_{\ell,\pm1} = \pm\frac{\Omega}{2}\sqrt{\pi\ell(\ell+1)(2\ell+1)}\,\frac{R^{\ell+1}(-1)^{\frac{\ell+1}{2}}}{1+(2\ell+1)(L_s/R)}\cdot\frac{(\ell-2)!!}{(\ell+1)!!}, \quad \ell \text{ odd.} \tag{A.43}$$

The condition of a flat 'interface' reads

$$g_{10}(r)K_{10}\left[\partial_\vartheta P_{10}(\cos\vartheta)\right]_{\vartheta=(\pi/2)} + \sum_{m=\pm1}\sum_{\substack{\ell=1\\\ell\text{ odd}}}^{\infty} g_{\ell m}(r)K_{\ell m}\left[\partial_\vartheta P_{\ell m}(\cos\vartheta)\right]_{\vartheta=(\pi/2)}$$

$$+ \sum_{m=\pm1}\sum_{\substack{\ell=2\\\ell\text{ even}}}^{\infty} m h_{\ell m}(r)K_{\ell m}P_{\ell m}(0) = 0. \tag{A.44}$$

The sums vanish completely due to properties of the Legendre functions at zero [38], so that only the first term remains, giving

$$b_{10}\left[1 + \frac{1}{2}\frac{R^3}{r^3}\right] + \frac{c_{10}}{2r}\left[1 + \frac{R^2}{r^2}\right] = 0. \tag{A.45}$$

Since this equation must be valid for arbitrary r it follows $b_{10} = 0 = c_{10}$. In order to evaluate the force condition

$$F_x = R^2\int_0^{2\pi}d\varphi\int_0^{\pi/2}d\vartheta\,\sin\vartheta\left[\sigma_{rr}(R)\sin\vartheta\cos\varphi + \sigma_{r\vartheta}(R)\cos\vartheta\,\cos\varphi - \sigma_{r\varphi}(R)\sin\varphi\right] = 0 \tag{A.46}$$

the following integrals are needed:

$$\int_0^{\pi/2}d\vartheta\,\sin\vartheta\left[\frac{1}{\sin\vartheta} + \cos\vartheta\,\partial_\vartheta\right]P_{\ell1}(\cos\vartheta) = \int_0^{\pi/2}d\vartheta\,\sin^2\vartheta\,P_{\ell1}(\cos\vartheta) = \frac{4}{3}\delta_{\ell1}. \tag{A.47}$$

Then the last coefficients are given by

$$b_{1,\pm1} = \mp\frac{\Omega R}{1+2(L_s/R)}\sqrt{\frac{\pi}{6}}. \tag{A.48}$$

Appendix B. Resulting flow fields for the liquid half-sphere model

$$v_r^{(i)} = \frac{3}{4}\frac{\mathfrak{M}R}{2\eta^{(o)}+3\eta^{(i)}}\sin\vartheta\,\cos\varphi\left[\frac{r^2}{R^2} - 1\right]$$

$$+ \frac{\mathfrak{M}R\cos\varphi}{\eta^{(o)}+\eta^{(i)}}\sum_{\substack{\ell=3\\\ell\text{ odd}}}^{\infty}P_{\ell1}(\cos\vartheta)\frac{r^{\ell-1}}{R^{\ell-1}}(-1)^{\frac{\ell-1}{2}}\left[\frac{r^2}{R^2} - 1\right]\frac{(\ell-2)!!}{(\ell+1)!!}, \tag{B.1}$$

$$v_r^{(o)} = \frac{1}{2} \frac{\mathfrak{M}R}{2\eta^{(o)} + 3\eta^{(i)}} \, \sin\vartheta \cos\varphi \left[1 - \frac{R^3}{r^3}\right]$$

$$+ \frac{\mathfrak{M}R \cos\varphi}{\eta^{(o)} + \eta^{(i)}} \sum_{\substack{\ell=3 \\ \ell \text{ odd}}}^{\infty} P_{\ell 1}(\cos\vartheta) \frac{R^\ell}{r^\ell} \left[1 - \frac{R^2}{r^2}\right] (-1)^{\frac{\ell-1}{2}} \frac{(\ell-2)!!}{(\ell+1)!!}, \tag{B.2}$$

$$\begin{pmatrix} v_\vartheta^{(i)} \\ v_\varphi^{(i)} \end{pmatrix} = \frac{3}{4} \frac{\mathfrak{M}R}{2\eta^{(o)} + 3\eta^{(i)}} \begin{pmatrix} \cos\varphi \cos\vartheta \\ -\sin\varphi \end{pmatrix} \left[2\frac{r^2}{R^2} - 1\right] + \frac{\mathfrak{M}R}{\eta^{(o)} + \eta^{(i)}} \begin{pmatrix} \cos\varphi \, \partial_\vartheta \\ -\sin\varphi / \sin\vartheta \end{pmatrix}$$

$$\times \sum_{\substack{\ell=3 \\ \ell \text{ odd}}}^{\infty} P_{\ell 1}(\cos\vartheta) \frac{r^{\ell-1}}{R^{\ell-1}} \left[\frac{(\ell+3)}{(\ell+1)} \frac{r^2}{R^2} - 1\right] \frac{(-1)^{\frac{\ell-1}{2}}}{\ell} \frac{(\ell-2)!!}{(\ell+1)!!} + 2\mathfrak{M}R$$

$$\times \begin{pmatrix} -\cos\varphi / \sin\vartheta \\ \sin\varphi \, \partial_\vartheta \end{pmatrix} \sum_{\substack{\ell=2 \\ \ell \text{ even}}}^{\infty} \frac{P_{\ell 1}(\cos\vartheta) \, (-1)^{(\ell/2)}}{(\ell+2)\eta^{(o)} + (\ell-1)\eta^{(i)}} \frac{r^\ell}{R^\ell} \frac{(2\ell+1)(\ell-3)!!}{\ell(\ell+1)(\ell+2)!!}, \tag{B.3}$$

$$\begin{pmatrix} v_\vartheta^{(o)} \\ v_\varphi^{(o)} \end{pmatrix} = \frac{1}{2} \frac{\mathfrak{M}R}{2\eta^{(o)} + 3\eta^{(i)}} \begin{pmatrix} \cos\varphi \cos\vartheta \\ -\sin\varphi \end{pmatrix} \left[1 + \frac{1}{2}\frac{R^3}{r^3}\right] + \frac{\mathfrak{M}R}{\eta^{(o)} + \eta^{(i)}} \begin{pmatrix} \cos\varphi \, \partial_\vartheta \\ -\sin\varphi / \sin\vartheta \end{pmatrix}$$

$$\times \sum_{\substack{\ell=3 \\ \ell \text{ odd}}}^{\infty} P_{\ell 1}(\cos\vartheta) \frac{R^\ell}{r^\ell} \left[(2-\ell) + \ell\frac{R^2}{r^2}\right] \frac{(-1)^{\frac{\ell-1}{2}}}{\ell(\ell+1)} \frac{(\ell-2)!!}{(\ell+1)!!} + 2\mathfrak{M}R$$

$$\times \begin{pmatrix} -\cos\varphi / \sin\vartheta \\ \sin\varphi \, \partial_\vartheta \end{pmatrix} \sum_{\substack{\ell=2 \\ \ell \text{ even}}}^{\infty} \frac{P_{\ell 1}(\cos\vartheta) \, (-1)^{(\ell/2)}}{(\ell+2)\eta^{(o)} + (\ell-1)\eta^{(i)}} \frac{R^{\ell+1}}{r^{\ell+1}} \frac{(2\ell+1)(\ell-3)!!}{\ell(\ell+1)(\ell+2)!!}. \tag{B.4}$$

References

[1] Rosensweig R E 1985 *Ferrohydrodynamics* (Cambridge: Cambridge University Press)
[2] Bacri J-C, Cebers A and Perzynski R 1994 *Phys. Rev. Lett.* **72** 2705
[3] Cebers A and Lacis S 1995 *Braz. J. Phys.* **25** 101
[4] Morozov K I and Lebedev A V 1997 *Sov. Phys.—JETP* **65** 160
[5] Morozov K I 2000 *JETP* **85** 728
[6] Sandre O, Broways J, Perzynski R, Bacri J-C, Cabuil V and Rosensweig R E 1999 *Phys. Rev.* E **59** 1736
[7] Cebers A 2002 *Phys. Rev.* E **66** 061402
[8] Morozov K I and Lebedev A V 2000 *JETP* **91** 1029
[9] Lebedev A V, Engel A, Morozov K I and Bauke H 2003 *New J. Phys.* **5** 57
[10] Blums E, Cebers A and Maiorov M 1997 *Magnetic Fluids* (Berlin: Walter de Gruyter)
[11] Krauss R, Liu M, Reimann B, Richter R and Rehberg I 2005 *Appl. Phys. Lett.* **86** 024102
[12] Krauss R, Liu M, Reimann B, Richter R and Rehberg I 2006 *New J. Phys.* **8** 18
[13] Bönnemann H, Brijoux W, Brinkmann R, Matoussevitch N and Waldöfner N 2003 *German Patent* DE 10227779.6.
[14] Sterr V 2007 *Diploma Thesis* University of Oldenburg

[15] Huh C and Scriven L E 1971 *J. Colloid Interface Sci.* **35** 85
[16] de Gennes P-G 1986 *Colloid Polymer Sci.* **264** 463
[17] Navier C-L 1823 *Mém. Acad. Sci. Inst. France* **6** 389
[18] Dussan V E B 1976 *J. Fluid Mech.* **77** 665
[19] Pismen L M and Rubinstein B Y 2001 *Langmuir* **17** 5265
[20] Huh C and Mason S G 1977 *J. Fluid Mech.* **81** 401
[21] Hocking L M 1977 *J. Fluid Mech.* **79** 209
[22] Cox R G 1986 *J. Fluid Mech.* **168** 169
[23] O'Neill M E, Ranger K B and Brenner H 1986 *Phys. Fluids* **29** 913
[24] Denn M M 2001 *Annu. Rev. Fluid Mech.* **33** 265
[25] Joseph P and Tabeling P 2005 *Phys. Rev.* E **71** 035303
[26] Schmatko T, Hervet H and Leger L 2005 *Phys. Rev. Lett.* **95** 244501
[27] Fetzer R, Rauscher M, Münch A, Wagner B and Jacobs K 2006 *Europhys. Lett.* **4** 638
[28] Sorokin V S 1948 *Zh. Eksp. Teor. Fiz.* **18** 228
[29] Morse P M and Feshbach H 1953 *Methods of Theoretical Physics* vol 2 (New York: McGraw-Hill) chapter 13
[30] Landau L D and Lifschitz E M 1991 *Lehrbuch der Theoretischen Physik* vol 6, 5th edn (Berlin: Akademie Verlag)
[31] Landau L D and Lifschitz E M 1990 *Lehrbuch der Theoretischen Physik* vol 8 *Elektrodynamik der Kontinua* 5th edn (Berlin: Akademie Verlag)
[32] Shliomis M I 1974 *Sov. Phys.—Usp.* **17** 153
[33] Pamme N 2006 *Lab Chip* **6** 24
[34] Nguyen N-T, Ng K M and Huang X 2006 *Appl. Phys. Lett.* **89** 052509
[35] Thorsen T, Roberts R W, Arnold F H and Quake S R 2001 *Phys. Rev. Lett.* **86** 4163
[36] Pekas N, Porter M D, Tondra M, Popple A and Jander A 2004 *Appl. Phys. Lett.* **85** 4783
[37] Cohen-Tannoudji C, Diu B and Laloë F 1999 *Quantenmechanik* 2nd edn (Berlin: de Gruyter)
[38] Abramowitz M and Stegun I A (ed) 1970 *Handbook of Mathematical Functions* 14th edn (New York: Dover)